Vegetable Research

ARTICLE

Open Access

https://doi.org/10.48130/vegres-0026-0030

Vegetable Research **2026**, 6: e037

Synergistic physiological and transcriptomic responses in ginger (*Zingiber officinale* Roscoe) with different saline–alkali sensitivities under salt–alkali stress

Hanqing Liu[1], Song Gao[2], Zijing Chen[1], Di Wang[1], Miaohong Liu[1], Yuwen Kong[1], Xianxiang Li[1], Junqi Ai[1], Yao Lv[1,3*] and Kun Xu[1,3*]

[1] *College of Horticulture Science and Engineering, Shandong Agricultural University, Taian 271018, China*
[2] *College of Horticulture and Landscape Architecture, Yangzhou University, Yangzhou 225009, China*
[3] *Key Laboratory of Biology of Horticultural Crops in Huanghuai Region, Ministry of Agriculture and Rural Affairs, Taian 271018, China*
* Correspondence: lvyao@sdau.edu.cn (Lv Y); xukun@sdau.edu.cn (Xu K)

Abstract

Salt–alkali land represents a crucial reserve of arable resources that urgently requires efficient utilization. To date, studies on the response of ginger (*Zingiber officinale* Roscoe) to salt–alkali stress remain limited. In this study, a simulated salt–alkali soil environment (pH 7.8, 0.3% salt content) was established to compare the physiological and transcriptomic responses of a tolerant ginger cultivar, '2404' (T), and a sensitive cultivar, '61' (S). The results showed that after 7 d of stress, chlorophyll *a* content and net photosynthetic rate decreased by 12.27% and 33.93% in Cultivar T, respectively, whereas those in Cultivar S decreased by 50.78% and 94.11%. Cultivar T rapidly and consistently accumulated proline and soluble sugars and showed significantly enhanced antioxidant enzyme activities. After 5 d of treatment, the activities of peroxidase (POD), catalase (CAT), and glutathione reductase (GR) in T were 64.94%, 93.14%, and 37.75% higher than those in S, respectively. Throughout the stress period, the reduced glutathione (GSH) content in T remained significantly higher than that in S, and after 10 d of treatment, the GSH content in S was 70.00% lower than that in T. Transcriptomic analysis and weighted gene co-expression network analysis identified nine hub genes, which could be regarded as the most promising candidate targets for future functional research in ginger. In conclusion, under salt–alkali stress, the salt–alkali-tolerant cultivar maintained higher photosynthetic capacity and exhibited robust antioxidant and osmotic adjustment abilities. This study provides a valuable reference for the screening and functional validation of salt–alkali tolerance genes in ginger.

Keywords: Ginger, Salt–alkali stress, DEGs, RNA-Seq, WGCNA

Citation: Liu H, Gao S, Chen Z, Wang D, Liu M, et al. 2026. Synergistic physiological and transcriptomic responses in ginger (*Zingiber officinale* Roscoe) with different saline–alkali sensitivities under salt–alkali stress. *Vegetable Research* 6: e037 https://doi.org/10.48130/vegres-0026-0030

Introduction

Soil salinization has emerged as a critical global challenge constraining sustainable agricultural development. The global extent of salt–alkali land exceeds 1.1 billion hectares, of which approximately 40% is classified as alkaline soil[1]. The ionic composition of natural salt–alkali soils is complex, typically containing Na^+, Ca^{2+}, Mg^{2+}, Cl^-, and SO_4^{2-}. Alkaline soils, in particular, are characterized by elevated pH resulting from high concentrations of HCO_3^- and CO_3^{2-}. The combined effects of salinity and alkalinity often induce more severe damage to crops, thereby constraining their growth and productivity[2]. Salt–alkali land, as a critically important reserve of arable land resources, plays a vital role in safeguarding global food security for a burgeoning population. However, salt–alkali stress represents a multifaceted stressor that adversely affects plants by disrupting the soil's physicochemical properties, constraining crop productivity, and impairing ecosystem functionality, thereby severely constraining agricultural production[3]. China is one of the world's major ginger (*Zingiber officinale* Roscoe)-producing regions. However, with the extension of continuous cropping years, most traditional production areas are increasingly confronted with soil salinization and rising pH levels. When ginger plants are subjected to salt–alkali stress, they exhibit typical foliar damage; in severe cases, yield losses can exceed 30%, thereby seriously constraining the green and sustainable development of the ginger industry[4].

Salt–alkali stress imposes osmotic stress and ion toxicity on plants, leading to physiological drought and impaired mineral nutrient uptake. This disruption subsequently triggers the overproduction of reactive oxygen species (ROS), resulting in secondary damage such as oxidative stress[5]. Leaves, as the primary sites of photosynthesis, are highly sensitive to salt–alkali stress. Such stress increases Na^+ accumulation and reduces K^+ content in the leaves, and the consequent imbalance in the Na^+/K^+ ratio disrupts both ionic and osmotic homeostasis, thereby inhibiting plant growth[6]. Initially, salt–alkali stress induces stomatal closure, thereby impeding CO_2 uptake and subsequently reducing the intercellular CO_2 concentration (C_i) and photosynthetic rate[7]. Concurrently, salt–alkali stress disrupts chloroplast structure and inhibits photosynthetic electron transport, thereby leading to a marked decline in photosynthetic efficiency[8]. ROS bursts induced by excess light energy also constitute a major factor limiting crops' productivity under salt–alkali stress[9].

To cope with salt–alkali stress, plants have evolved a suite of adaptive mechanisms primarily involving the reestablishment of ion homeostasis, the regulation of osmotic balance, and ROS scavenging[10]. With respect to ion homeostasis, plasma membrane-localized Na^+/H^+ antiporters (e.g., Salt Overly Sensitive 1) extrude excess Na^+ from the cytoplasm, whereas tonoplast-localized Na^+/H^+ antiporters (e.g., members of the Na^+/H^+ exchanger [NHX] family) sequester Na^+ into the vacuole. The coordinated action of these transporters is central to alleviating cytosolic ion toxicity[11].

© The Author(s)

https://doi.org/10.48130/vegres-0026-0030

Regarding osmotic regulation, salt–alkali stress induces the synthesis of osmolytes, such as proline and betaine, to maintain cellular osmotic balance. For instance, overexpression of *AtSIZ1* has been shown to promote the accumulation of proline and soluble sugars in *Arabidopsis thaliana*[12], and *SlWRKY42* regulates *SlP5CS1* to promote proline accumulation[13]. Concerning ROS scavenging, antioxidant enzyme systems, including superoxide dismutase (SOD) and peroxidase (POD), are activated to eliminate excess ROS[14], whereas antioxidants such as reduced glutathione (GSH) directly react with ROS[15]. Furthermore, plant hormone signaling, mitogen-activated protein kinase (MAPK) cascade pathways, heat shock protein-related pathways, and transcription factor families like MYB and WRKY play crucial roles in responding to salt–alkali stress[16]. Although the aforementioned mechanisms of ion homeostasis, osmotic adjustment, and ROS scavenging have been widely documented across various plant species, different plant taxa exhibit marked species-specific responses to saline–alkali stress. To date, studies on the response of Zingiberaceae plants to saline–alkali stress remain extremely scarce.

Ginger, an important economic crop with medicinal and edible value, is widely cultivated in China, the world's largest producer[17]. However, ginger is a shallow-rooted plant with roots that are highly sensitive to changes in the soil environment. The optimal soil pH for ginger growth ranges from 5.8 to 7.0, and its salinity tolerance threshold is approximately 0.35%, classifying it as a typical salt–alkali-sensitive crop[4]. To date, no study has reported on the dynamic physiological responses or conducted a comparative transcriptomic analysis of leaves between tolerant and sensitive ginger cultivars under salt–alkali stress. In this study, a salt–alkali-tolerant ginger germplasm was used as the experimental material, with a sensitive germplasm as the control. The objectives were to analyze the dynamic physiological differences between the tolerant and sensitive germplasm under salt–alkali stress and to identify hub modules and hub genes significantly associated with salt–alkali tolerance through transcriptomic analysis and weighted gene co-expression network analysis (WGCNA), thereby providing a reference for the screening and functional validation of salt–alkali tolerance genes in ginger. The hypotheses were as follows: (1) the tolerant cultivar maintains higher photochemical efficiency; (2) the tolerant cultivar accumulates substantial amounts of osmotic adjustment substances; (3) the tolerant cultivar exhibits higher antioxidant system activity; and (4) genes related to signal transduction and other pathways are significantly enriched in the tolerant cultivar. Therefore, a systematic elucidation of the molecular regulatory network governing salt–alkali tolerance in ginger would not only provide a theoretical foundation for expanding ginger cultivation on saline–alkali soils but also furnish key genetic resources and selection markers for stress-tolerant molecular breeding in *Zingiberaceae* crops, offering substantial practical value for industrial application.

Materials and methods

Experimental design

The experiment was conducted in 2025 at the Science and Technology Innovation Park of Shandong Agricultural University. The tested ginger materials comprised a salt–alkali-tolerant cultivar, '2404' (T), and a salt-sensitive cultivar, '61' (S) (Supplementary Table S1 and Supplementary Fig. S1). After sprouting, the ginger rhizomes were sown in plastic pots (height: 20 cm, diameter: 27 cm), each filled with 3.6 kg of soil. When the plants grew to approximately 60 cm in height, uniformly growing plants were selected and divided into control and treatment groups. The control groups received normal management. For the treatment groups, salt–alkali stress was applied by first adding neutral salts (NaCl: Na_2SO_4 = 1:1, w/w) at 0.3% of the dry soil weight, followed by irrigating with a 1 mol·L^{-1} KOH solution to adjust the soil pH to approximately 7.8. Consequently, four treatments were established: Tn (tolerant control), Ts (tolerant under salt–alkali stress), Sn (sensitive control), and Ss (sensitive under salt–alkali stress). Each treatment consisted of 24 plants, replicated four times. Sampling for relevant indicator measurements was performed at 1, 3, 5, 7, and 10 d after the treatment's initiation. For transcriptome sequencing analysis, the third fully expanded functional leaf from the top was collected at 1, 5, and 7 d after treatment; immediately frozen in liquid nitrogen; and stored at −80 °C until use. All samples were collected in triplicate.

Measurement items and methods

Chlorophyll content and photosynthesis/gas exchange parameters

On the seventh day of treatment, the third functional leaf from the top was sampled to determine chlorophyll content according to the method described by Gao et al.[18]. Photosynthetic parameters of the expanded functional leaves were measured using a Ciras-3 photosynthesis system (PP-Systems, USA). Each treatment was measured three times, and the average value was calculated as the final result.

Measurement of fast chlorophyll a fluorescence induction kinetics

On the seventh day of treatment, the fast chlorophyll *a* fluorescence induction kinetics curve was measured using an m-PEA fluorometer (Hansatech, UK). Following the method of Wang et al.[19], the leaves were dark-adapted for 30 min. The fluorescence signal was recorded from 10 μs to 1 s under a saturating pulse light (3,500 μmol·m^{-2}·s^{-1}) to plot the fast chlorophyll *a* fluorescence induction kinetics (OJIP) curve for subsequent analysis.

Measurement of chlorophyll fluorescence parameters

The chlorophyll fluorescence parameters of functional leaves were measured on the seventh day of treatment using a MINI-IMAGING-PAM chlorophyll fluorescence imaging system (Heinz Walz GmbH, Effeltrich, Germany).

Determination of malondialdehyde, H_2O_2, O_2^-, and osmolyte contents

Fresh leaf samples were collected at 1, 3, 5, 7, and 10 d after treatment initiation, washed with distilled water, dried, immediately frozen in liquid nitrogen, and stored at −80 °C. The contents of malondialdehyde (MDA), hydrogen peroxide (H_2O_2), and superoxide anion radicals (O_2^-) were measured according to the method of Liu et al.[20]. Soluble protein and soluble sugar contents were determined using the Coomassie Brilliant Blue method and the anthrone colorimetric method, respectively[21]. Proline content was assayed using the ninhydrin method[22].

Determination of antioxidant content and antioxidant enzyme activities

Fresh leaf samples collected at 1, 3, 5, 7, and 10 d after treatment were immediately frozen in liquid nitrogen and stored at −80 °C. The contents of GSH and oxidized glutathione (GSSG) were measured using commercial kits (Suzhou Comin Biotechnology Co., Ltd., China), and the GSH/GSSG ratio was calculated. The activities of SOD, POD, and catalase (CAT) were determined following the

method of Zafari et al.[23]. Glutathione reductase (GR) activity was assayed according to Guo et al.[24] by monitoring the decrease in absorbance at 340 nm.

Transcriptome analysis and quantitative real-time polymerase chain reaction-based validation

Transcriptome sequencing was performed by Beijing Novogene Co., Ltd. For simplicity of analysis, samples of the cultivar '2404' under control conditions (Day 0) and stress conditions at 1, 5, and 7 d were designated as T0, T1, T5, and T7, respectively. Similarly, samples of the cultivar '61' were designated as S0, S1, S5, and S7.

To obtain clean reads, we first verified sequence quality using FastQC (www.bioinformatics.babraham.ac.uk/projects/fastqc). All downstream analyses were based on high-quality clean data. The reads were aligned to the reference genome using HISAT2. Differentially expressed genes (DEGs) were identified using the R package DESeq2 with the criteria of $\log_2$ (fold change) > 1 or $\log_2$ (fold change) < −1 and statistical significance (p-value < 0.05). Finally, all DEGs were subjected to enrichment analysis using the Gene Onto logy (GO) (www.geneontology.org), SwissProt (www.expasy.ch/sprot), and Kyoto Encyclopedia of Genes and Genomes (KEGG) (www.genome.jp/kegg) databases. Nine DEGs were randomly selected from the transcriptome data for validation by quantitative real-time polymerase chain reaction (qRT-PCR). Gene-specific primers were designed using Primer Premier 6.0 software based on the coding sequences. *ZoRPII* was used as the internal reference gene[25]. The primer sequences are listed in Table 1. All procedures were performed with three biological replicates.

Weighted gene co-expression network analysis

WGCNA was performed using the fragments per kilobase of sequence per million mapped reads (FPKM) values on the BMKCloud platform (Beijing, China).

Statistical analysis

Sampling was carried out strictly following the principle of randomization. Each treatment consisted of three biological replicates, and the results are presented as mean ± standard deviation (SD). Before analysis, all data were tested and confirmed to meet the assumptions of a normal distribution and homogeneity of variances. One-way analysis of variance (ANOVA) was performed using DPS software, and the significance of differences among treatments was assessed by Duncan's new multiple range test at a significance level of $p < 0.05$. Basic data processing, calculations, and graphical visualization were carried out using Excel 2019 and R software.

Table 1. Primer sequences.

Gene name	Primer name	Primer sequence
ZoRPII	F	CTGCTGATGGATACGAATG
	R	CTGCCCAAGAGAATGAAAG
ZoPUB18	F	CGCCAGCAAGAACCTCTCCTTC
	R	GAATGCCGCCGCCATCTTCAT
ZoPMI1	F	GCGAGGAGGACCTAGCACTCAA
	R	GCACCACGGAACCCAAACCTTT
ZoD27	F	ATGCGTCGGGATGTGTGTCAAC
	R	TTCAATAGGCGGCGGCACTTG
ZoELIP1	F	TCATGCTTCGCAGGCTCCAGA
	R	TCCTCAGCTTGACACCTCACCG
ZoNAAT1	F	TGATTCAGGCAGCGGTTCCCA
	R	GTGGCATCGCAGTGGCTTGAT
ZoRTE1	F	CAGCCATACAGACACGCCGAAC
	R	TCAGGCAGGCAGCAACAAAGAC
ZoLNK1	F	TGCTGCTGCAAATGCTGAAGGT
	R	CGCGCTACAGACCGATCAATGG
ZoTCP13	F	CCAACACTCCTCCTGCCACTGA
	R	ACCTTGCTGTGCCGGTCCTT
ZoUVR8	F	CCAGTGCGGACAAGGGAGTACA
	R	GCCAGCAGCAACTCGTTGGAT

Results

Effects of salt–alkali stress on chlorophyll content and photosynthetic gas exchange parameters in ginger leaves

On Day 7 of salt–alkali stress treatment, the two ginger cultivars exhibited pronounced phenotypic differences in their leaves (Fig. 1b). Compared with the Tn control, the Ts plants showed reductions of 12.27%, 10.00%, 16.98%, and 11.41% in chlorophyll *a*, chlorophyll *b*, total chlorophyll (*a* + *b*), and carotenoid contents, respectively (Fig. 1a, c). By contrast, relative to Sn, the Ss plants displayed more severe declines of 50.78%, 56.31%, 51.92%, and 52.49% in chlorophyll *a*, chlorophyll *b*, total chlorophyll (*a* + *b*), and carotenoid contents, respectively (Fig. 1a, c). Regarding photosynthetic parameters, compared with Tn, the Ts plants exhibited decreases of 33.93%, 17.91%, 11.54%, and 16.20% in net photosynthetic rate (P_n), transpiration rate (T_r), water use efficiency (WUE), and stomatal conductance (G_s), respectively, whereas C_i increased by 22.12%. In the sensitive cultivar, compared with Sn, the Ss plants displayed drastic reductions of 94.11%, 71.59%, 79.47%, and 70.10% in P_n, T_r, WUE, and G_s, respectively, accompanied by a 42.55% increase in C_i.

Effects of salt–alkali stress on Photosystem II in ginger leaves

On Day 7 of salt–alkali stress, the OJIP (Fast Chlorophyll fluorescence induction curve/OJIP transient) transient curves exhibited marked alterations in both the tolerant and sensitive cultivars (Fig. 2a). Following normalization according to the formula $V_t = (F_t - F_0)/(F_m - F_0)$ (V_t: Relative variable fluorescence at time t, the corresponding normalized curves were obtained, F_t: Chlorophyll fluorescence at time t, F_0: Minimum [initial] fluorescence, F_m: Maximum fluorescence) (Fig. 2b). The amplitudes of the K–J and J–I phases in Ts were relatively small, whereas the amplitudes of the O–K, K–J, and J–I phases in Ss were substantially greater than those in Ts. Differential normalization, calculated as $\Delta V_t = V_{st} - V_{ck} = \Delta(F_t - F_0)/(F_m - F_0)$ (ΔV_t: Differential relative variable fluorescence, calculated as $V_{st} - V_{ck}$, V_{st}: Relative variable fluorescence under salt-alkali stress, V_{ck}: Relative variable fluorescence of the non-stressed control), yielded a double-peak curve (Fig. 2c). Under salt–alkali stress, the peaks were primarily evident during the O–K and K–J phases. Compared with their respective nonstressed controls, both Ts and Ss displayed increased values of V_k (Relative variable fluorescence at the K-step), V_j (Relative variable fluorescence at the J-step), and V_i (Relative variable fluorescence at the I-step). However, the major difference between the two cultivars was seen in V_k and V_j, with the increases being significantly greater in Ss than in Ts (Supplementary Fig. S1). Chlorophyll fluorescence imaging revealed that on Day 7 of stress, Ts exhibited a deeper coloration in the F_v/F_m image, whereas the F_v/F_m image of Ss appeared light blue or even contained greenish areas (Fig. 2e). The false color representing Y(II) in Ts was lighter

https://doi.org/10.48130/vegres-0026-0030

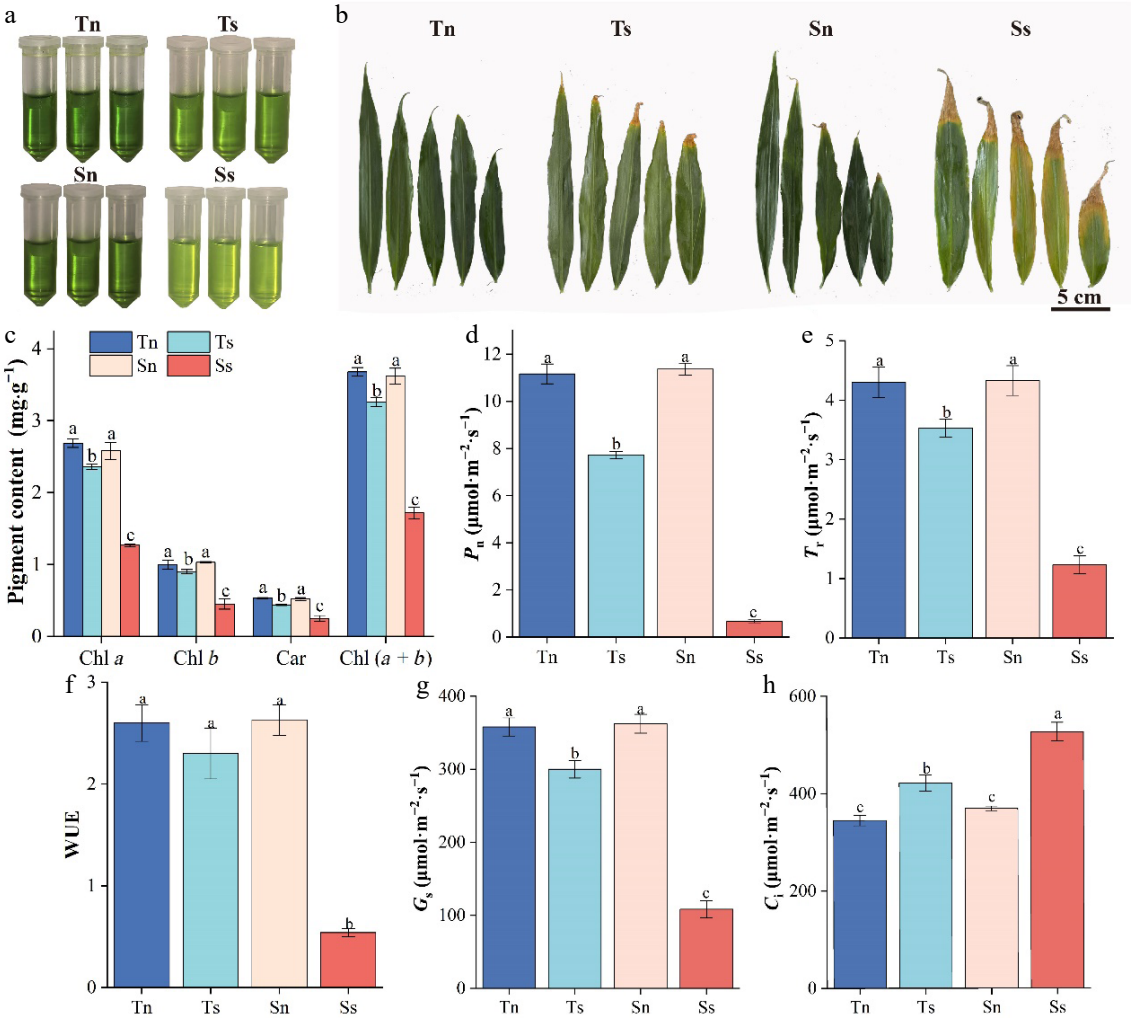


Fig. 1 Morphology, pigment content, and photosynthetic gas exchange parameters of ginger leaves under salt–alkali stress (7 d). (a) Leaf pigment extract. (b) Leaf phenotype. (c) Pigment content. (d)–(h) Photosynthetic gas exchange parameters. Data are presented as the mean ± standard deviation (SD) (n = 3). Different lowercase letters indicate significant differences among different treatments ($p < 0.05$, one-way analysis of variance with Tukey's multiple comparison test).

compared with Tn, whereas the Y(II) image of Ss displayed a yellowish-brown hue. Quantitative analysis showed that compared with Tn, Ts experienced decreases of 7.67%, 20.53%, and 7.74% in F_v/F_m, Y(II), and qP, respectively, accompanied by a 29.18% increase in Y(NPQ). By contrast, compared with Sn, Ss exhibited more pronounced reductions of 29.62%, 59.01%, and 55.56% in F_v/F_m, Y(II), and qP (Photochemical quenching), respectively, although Y (NPQ) (Quantum yield of regulated non-photochemical energy loss in PSII) increased by 4.22% (Fig. 2d).

Effects of salt–alkali stress on the accumulation of osmolytes in ginger leaves

With increasing duration of salt–alkali stress, Ts rapidly accumulated substantial amounts of proline within the first 5 d, after which the level gradually stabilized (Fig. 3a). In contrast, the proline content in Ss increased slowly during the initial 3 d, peaked, and subsequently declined after Day 5 (Fig. 3a). Similarly, the soluble sugar content in Ts progressively increased throughout the stress period and eventually reached a plateau (Fig. 3b). For Ss, soluble sugar content gradually rose, peaked on Day 3, and thereafter declined (Fig. 3b). The soluble protein content in Ts gradually increased with prolonged stress, reached its maximum on Day 5, and then gradually decreased; nevertheless, it remained higher than that in Tn (Fig. 3c). Conversely, the soluble protein content in Ss progressively declined over time. Compared with Sn, the soluble protein content in Ss was reduced by 58.80% at 10 d after the treatment's initiation (Fig. 3c).

Effects of salt–alkali stress on the antioxidant system in ginger leaves

With prolonged salt–alkali stress, MDA content progressively increased in both ginger cultivars. However, in the tolerant cultivar under stress (Ts), MDA content began to stabilize after Day 5. The most pronounced difference between the two cultivars was observed on Day 10, with the sensitive cultivar under stress (Ss) exhibiting an MDA content 40.13% higher than that of Ts (Fig. 4a). Hydrogen peroxide (H_2O_2) content in Ts reached its peak on Day 5 of treatment and subsequently declined, whereas in Ss, it continued to rise with extended stress duration. By Day 10, the H_2O_2 content in Ss was 152.45% higher than that in Ts (Fig. 4b). A similar trend was observed for superoxide anion (O_2^-) content, with Ss showing a 74.50% higher O_2^- content compared with Ts on Day 10 (Fig. 4c). Salt–alkali stress differentially affected antioxidant enzyme

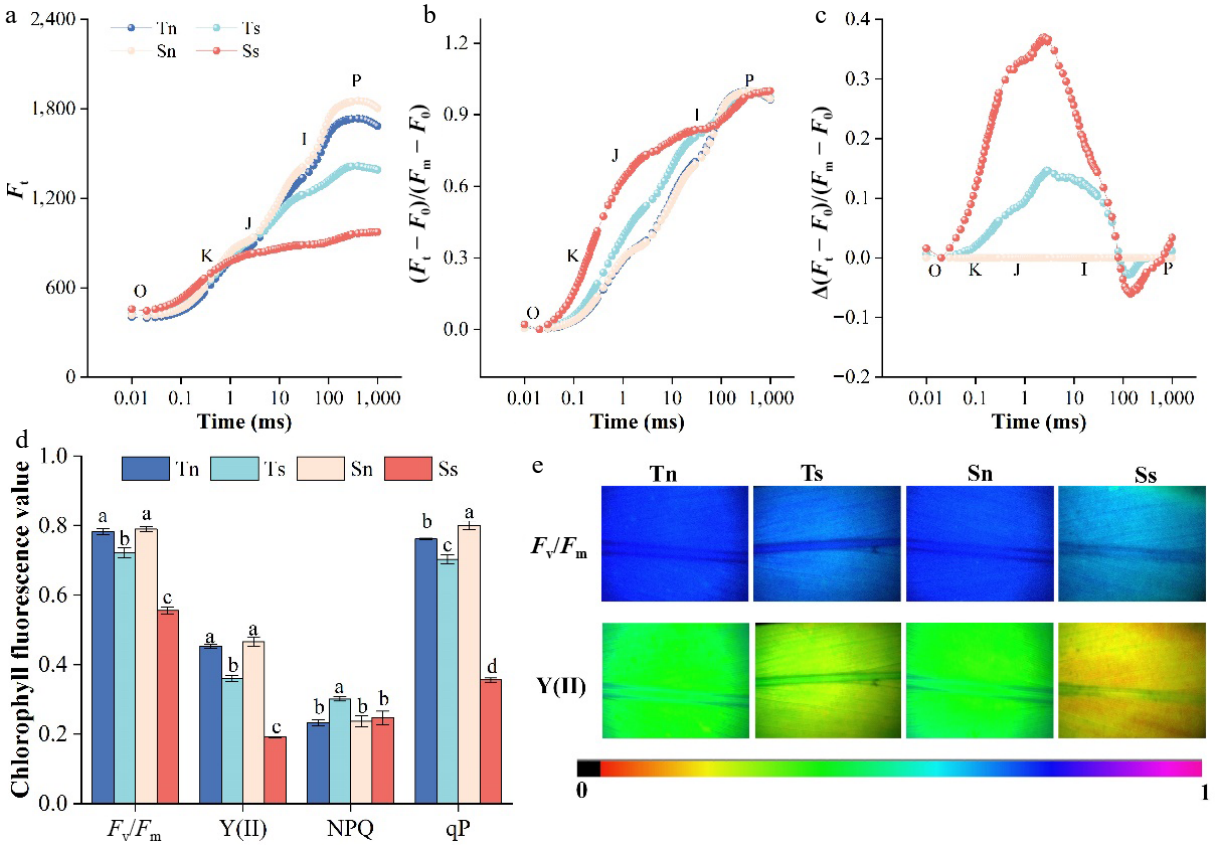


Fig. 2 Effect of salt–alkali stress on Photosystem II (PSII) of leaves in two ginger varieties (7 d). (a)–(c) Chlorophyll *a* transient fluorescence curves. (d) Chlorophyll fluorescence parameters. (e) Fluorescence images. Data are presented as the mean ± SD (n = 3). Different lowercase letters indicate significant differences among different treatments (p < 0.05, one-way ANOVA with Tukey's multiple comparison test).

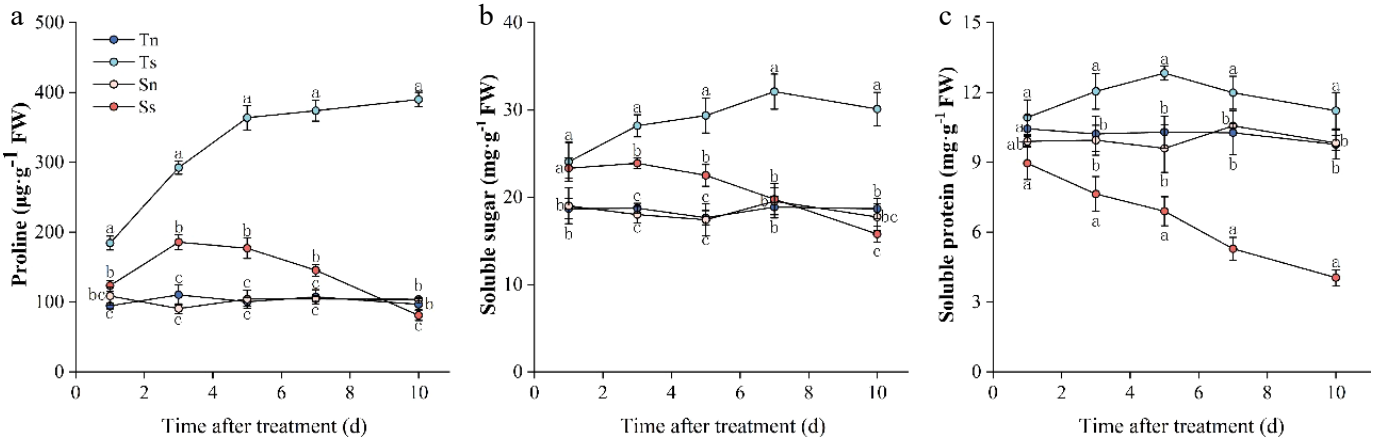


Fig. 3 Changes in proline (a), soluble sugar (b), and soluble protein contents (c) in the leaves of two ginger varieties under salt–alkali stress. Data are presented as the mean ± SD (n = 3). Different lowercase letters indicate significant differences among different treatments on the same day of stress (p < 0.05, one-way ANOVA with Tukey's multiple comparison test).

activities in the two cultivars. SOD activity in Ts increased rapidly and gradually stabilized after Day 3. In contrast, SOD activity in Ss increased slowly, peaked on Day 5, and then declined sharply thereafter (Fig. 4d). The responses of POD, CAT, and GR activities to stress followed patterns similar to that of SOD. On Day 5 of treatment, the activities of POD, CAT, and GR in Ts were significantly higher than those in Ss by 64.94%, 93.14%, and 37.75%, respectively (Figs. 4e, f and 5a).

Changes in reduced GSH content in both Ts and Ss exhibited an initial increase followed by a subsequent decrease. However, the GSH content in Ts remained substantially higher than that in Ss throughout the stress period. By Day 10, the GSH content in Ss was 70.00% lower than that in Ts (Fig. 5b). GSSG content in Ts showed a slight increase on Day 1, after which it gradually returned to stable levels. In contrast, GSSG content in Ss progressively increased; by Day 10 of treatment, it was 56.90% higher than that in Ts (Fig. 5c). With prolonged salt–alkali stress, the GSH/GSSG ratio in Ts gradually

https://doi.org/10.48130/vegres-0026-0030

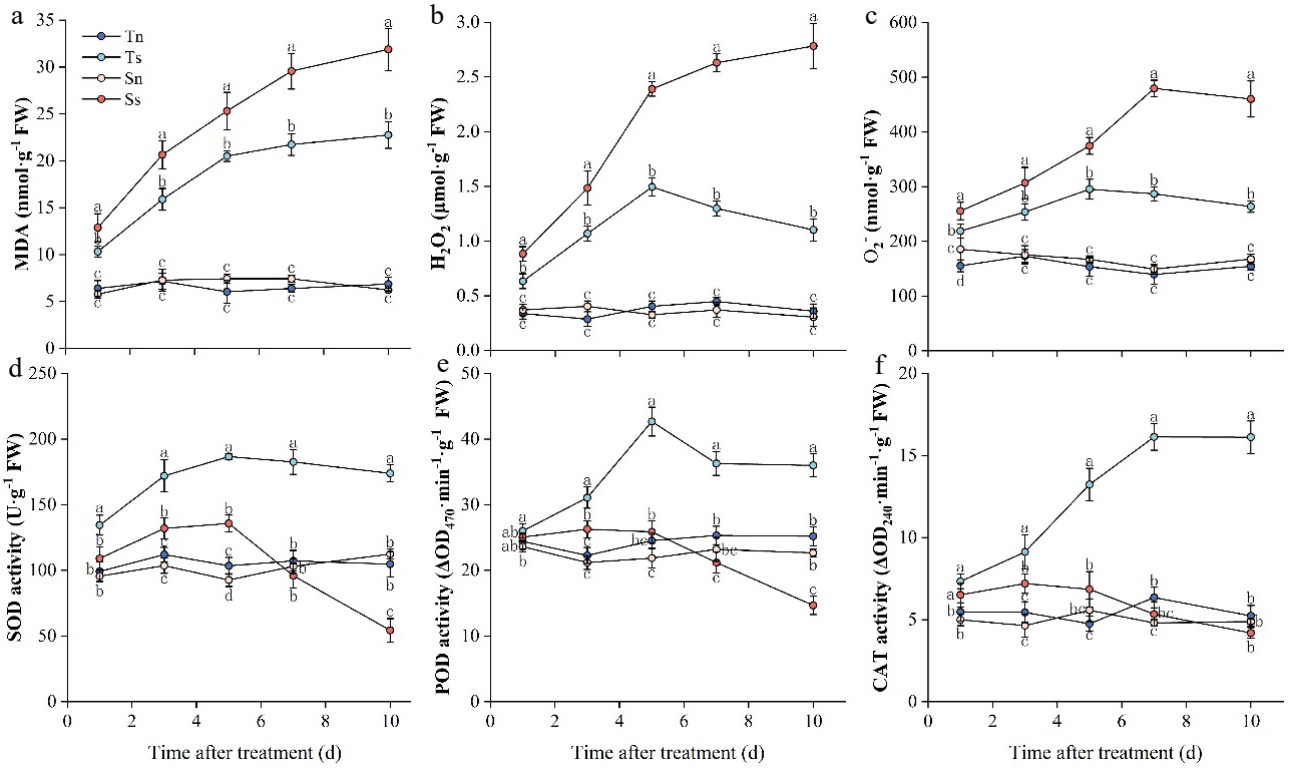


Fig. 4 Changes in (a) MDA, (b) H_2O_2, and (c) O_2^- content in leaves of two ginger varieties under salt–alkali stress. Changes in (d) SOD, (e) POD, and (f) CAT enzyme activities. Data are presented as the mean ± SD (n = 3). Different lowercase letters indicate significant differences among different treatments on the same day of stress (p < 0.05, one-way ANOVA with Tukey's multiple comparison test).

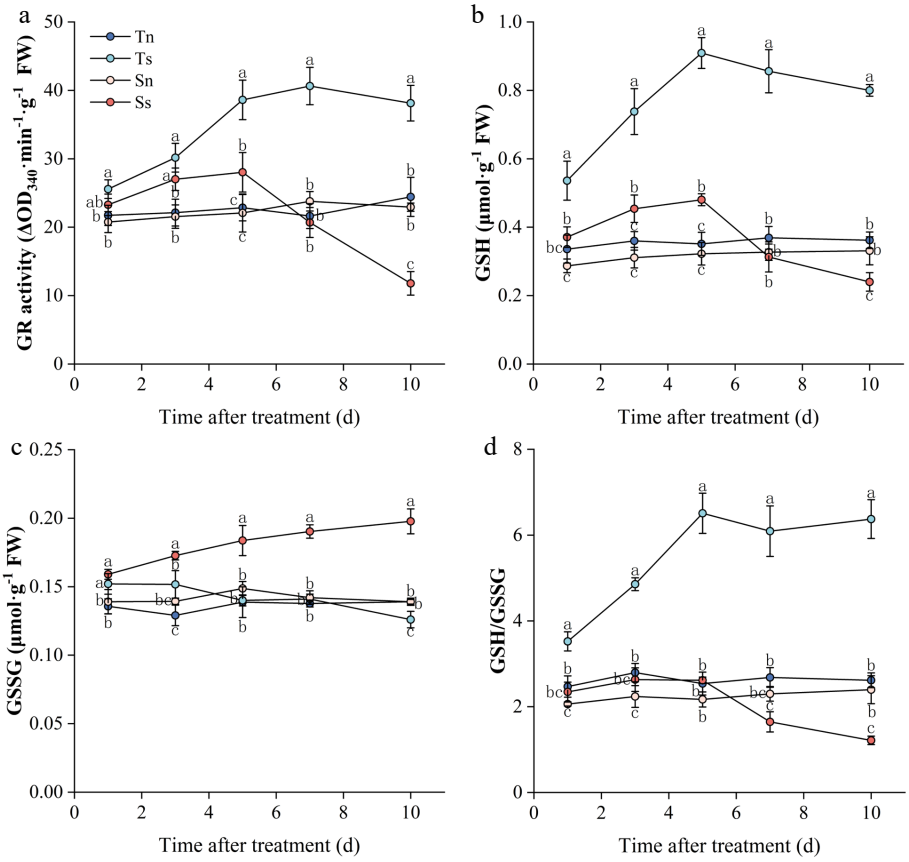


Fig. 5 (a) Changes in GR enzyme activity in the leaves of two ginger varieties under salt–alkali stress. Changes in (b) GSH, (c) GSSG, and (d) GSH/GSSG ratio. Data are presented as the mean ± SD (n = 3). Different lowercase letters indicate significant differences among different treatments on the same day of stress (p < 0.05, one-way ANOVA with Tukey's multiple comparison test).

increased, peaked on Day 5, and then slightly declined. In Ss, although the GSH/GSSG ratio exhibited a modest increase during the first 5 d of stress, it began to decline after Day 5, eventually falling below control levels. By Day 10 of stress, the GSH/GSSG ratio in Ts was 424.96% higher than that in Ss (Fig. 5d).

Correlation analysis and principal component analysis of physiological parameters under salt–alkali stress on Day 7

On Day 7 of salt–alkali stress, correlation analysis of the 26 physiological parameters showed that photosynthetic traits (chlorophyll, P_n, G_s, F_v/F_m, etc.) were positively correlated with each other ($r > 0.85$) and negatively correlated with C_i, MDA, H_2O_2, and O_2^- ($r < -0.80$). MDA, H_2O_2, and O_2^- were positively correlated with each other ($r > 0.85$) (Supplementary Fig. S2). In the principal component analysis (PCA) biplot, where the first two principal components (PCs) explain 74.3% and 15.8% of the variance, respectively, the stressed tolerant cultivar (Ts) was located in the positive PC1 and the negative PC2 region, close to proline and some antioxidant enzymes; the stressed sensitive cultivar (Ss) fell in the positive region of both PC1 and PC2, near O_2^-, MDA, and C_i; the control groups (Tn, Sn) were situated in the negative PC1 region (Supplementary Fig. S3).

Analysis of DEGs in tolerant and sensitive ginger cultivars under salt–alkali stress

To elucidate the molecular mechanisms underlying salt–alkali tolerance in ginger, DEGs were analyzed using leaf samples collected at different time points under salt–alkali stress, with the untreated control (0 d) serving as the reference. DEGs were identified according to the criteria of $|\log_2$ (fold change)$| \geq 1$ and false discovery rate (FDR) < 0.05. The results showed that in the sensitive cultivar (S), in total, 6,415 (3,168 upregulated/3,247 downregulated), 9,331 (4,185 upregulated/5,146 downregulated), and 8,642 (3,654 upregulated/4,988 downregulated) DEGs were identified at 1, 5, and 7 d of stress, respectively. In the tolerant cultivar (T), 6,791 (2,729 upregulated/4,062 downregulated), 6,271 (2,689 upregulated/3,582 downregulated), and 5,264 (2,448 upregulated/2,816 downregulated) DEGs were detected at the corresponding time points (Fig. 6a). PCA indicated good reproducibility among biological replicates (Fig. 6b). Pairwise comparisons revealed that the comparisons S0 vs S1, S0 vs S5, and S0 vs S7 contained 1,036, 2,687, and 2,808 unique DEGs, respectively. Similarly, the comparisons T0 vs T1, T0 vs T5, and T0 vs T7 contained 1,788, 1,567, and 1,492 unique DEGs, respectively. Furthermore, across all three time points (1, 5, and 7 d), a common set of 2,373 DEGs was consistently identified in Cultivar T under stress.

Functional enrichment analysis of DEGs

To investigate the potential functions of the DEGs, GO enrichment analysis was performed for both ginger cultivars, encompassing the cellular component (CC), biological process (BP), and molecular function (MF) categories (Supplementary Fig. S4). For the sensitive cultivar (S), the comparisons S0 vs S1, S0 vs S5, and S0 vs S7 showed enrichment of 47, 914, and 1,345 DEGs in CC; 2,631, 2,852, and 2,217 DEGs in BP; and 889, 768, and 368 DEGs in MF, respectively. For the tolerant cultivar (T), the comparisons T0 vs T1, T0 vs T5, and T0 vs T7 revealed enrichment of 255, 1,209, and 772 DEGs in CC; 2,227, 1,810, and 1,462 DEGs in BP; and 996, 946, and 1,354 DEGs in MF, respectively. In the GO enrichment

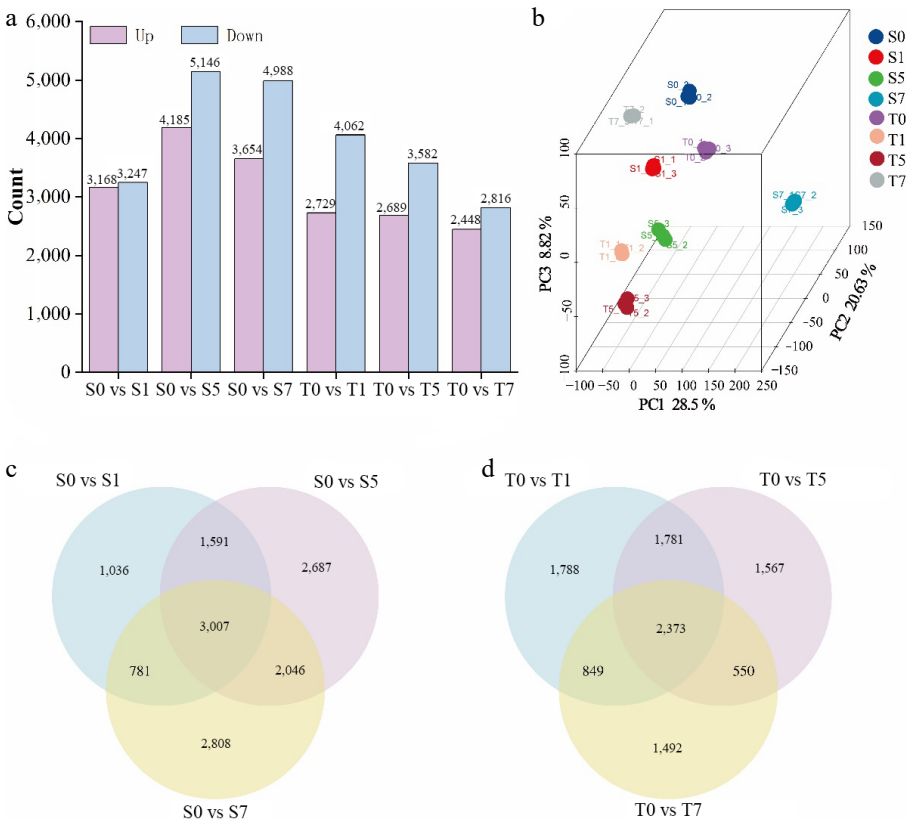


Fig. 6 Analysis of DEGs under salt–alkali stress in different comparison groups. (a) Number of upregulated and downregulated genes in different comparison groups. (b) PCA among samples. (c) Venn diagram of DEGs in Variety S. (d) Venn diagram of DEGs in Variety T.

https://doi.org/10.48130/vegres-0026-0030

analysis, genes enriched in the CC category for both cultivars were primarily associated with photosynthetic structures, including the photosynthetic membrane, chloroplast membrane, and thylakoid membrane. In Cultivar S, the top two enriched BP terms at 1, 5, and 7 d of treatment were 'response to abiotic stress' and 'response to oxygen-containing compounds'. In contrast, the number of genes enriched in these two BP terms in Cultivar T decreased with prolonged stress duration. For the MF category, both cultivars showed significant enrichment in terms such as endonuclease activity, nuclease activity, and hydrolase activity acting on ester bonds. Notably, in the tolerant cultivar (T), additional enrichment was observed for genes related to inorganic anion transmembrane transporter activity and dicarboxylic acid transmembrane transporter activity.

To further elucidate the pathways involved in ginger's response to salt–alkali stress, KEGG enrichment analysis was conducted on the DEGs from both cultivars (Fig. 7). The salt-sensitive cultivar (S) was enriched in 12 metabolic pathways, whereas the tolerant cultivar (T) was enriched in five pathways. Three pathways, namely 'metabolism of xenobiotics by cytochrome P450', 'alpha-linolenic acid metabolism', and 'ferroptosis', were enriched in both cultivars. Pathways such as 'thiamine metabolism' and 'methane metabolism' were exclusively enriched in Cultivar T. These shared and unique pathways are likely associated with ginger's resistance to salt–alkali stress. In contrast, pathways including 'glycerolipid metabolism', 'galactose metabolism', 'photosynthesis – antenna proteins', 'glyoxylate and dicarboxylate metabolism', 'fatty acid degradation', and 'tropane, piperidine, and pyridine alkaloid biosynthesis' were exclusively enriched in Cultivar S. These pathways may be related to the damage inflicted by salt–alkali stress on ginger.

Validation of gene expression

To verify the reliability of the transcriptome sequencing data, nine DEGs were randomly selected for qRT-PCR analysis (Supplementary Fig. S5). For all nine genes, the trends of up- or down-regulation were consistent between the RNA sequencing (RNA-seq) and qRT-PCR results. These findings confirm the accuracy of the expression patterns detected by RNA-seq.

WGCNA-based gene co-expression network analysis and identification of hub genes

WGCNA was performed using FPKM values with a cutoff >1, a coefficient of variation ≥ 0.5, a soft-thresholding power of 8, and a minimum module size of 30 genes. A gene dendrogram was constructed, based on the topological overlap matrix (TOM), and the dynamic tree cut algorithm was applied to identify and subsequently merge similar modules. This process yielded 17 distinct co-expression modules (Fig. 8). Among these, the ME-pale turquoise and ME-sienna-3 modules showed strong positive correlations with S1 (sensitive cultivar, Day 1). The ME-dark magenta module was highly correlated with S5, and the ME-light green module was strongly associated with S7. For the tolerant cultivar, the ME-cyan and ME-orange red-4 modules were highly positively correlated with T1, the ME-yellow green module with T5, and the ME-dark turquoise module with T7. Notably, the ME-medium purple-3

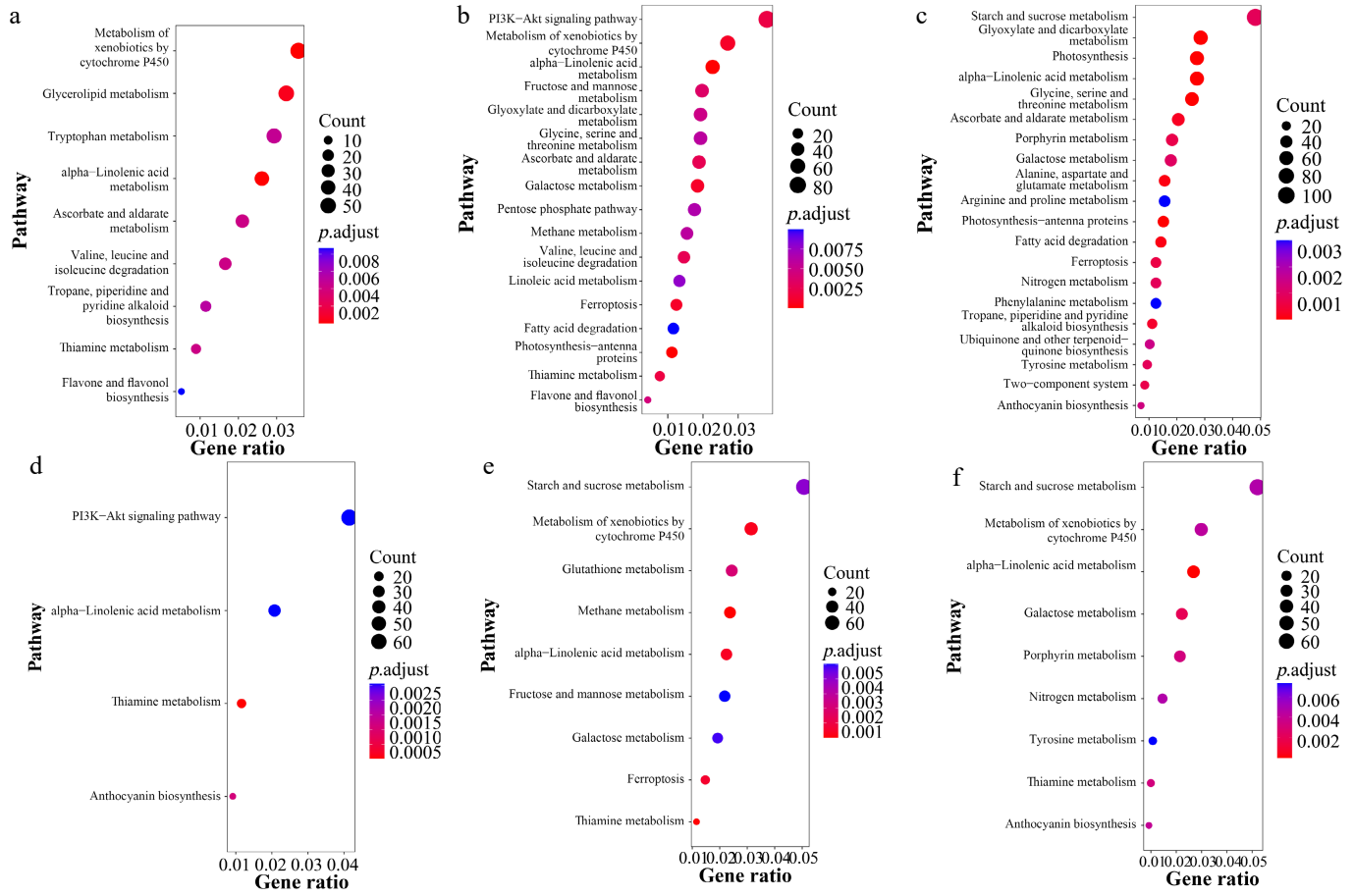


Fig. 7 KEGG enrichment analysis of DEGs in two ginger varieties: (a) S0 vs S1, (b) S0 vs S5, (c) S0 vs S7, (d) T0 vs T1, (e) T0 vs T5, and (f) T0 vs T7.

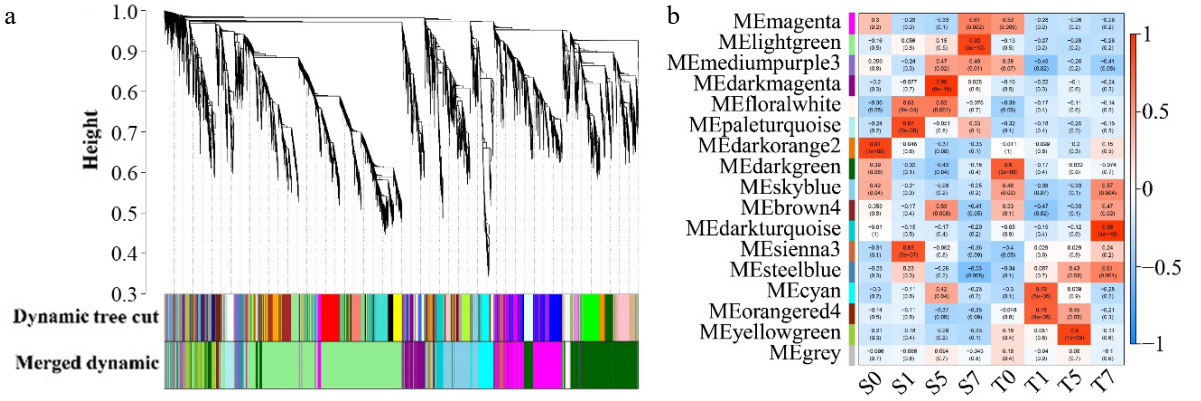


Fig. 8 (a) Gene clustering tree and module partitioning. (b) Correlation heatmap between gene co expression network modules and different samples. Gene clustering dendrogram and module-trait association heatmap.

module exhibited a positive correlation with S7 but a negative correlation with T7, suggesting it may contain genes that negatively regulate saline–alkali tolerance.

To elucidate the functional characteristics of genes within the key modules, KEGG enrichment analysis was performed on the hub genes from three modules highly positively correlated with the tolerant cultivar under stress (ME-cyan, ME-yellow green, and ME-dark turquoise) as well as from the ME-medium purple-3 module (Fig. 9). Key genes in the ME-cyan module were significantly enriched in 'protein processing in endoplasmic reticulum' and the 'PI3K–Akt signaling pathway' (Fig. 9a). Hub genes in the ME-yellow green module were notably enriched in 'amino sugar and nucleotide sugar metabolism' and 'fructose and mannose metabolism' (Fig. 9b). In the ME-dark turquoise module, key genes were significantly enriched in 'α-linolenic acid metabolism', 'plant hormone signal transduction', and the 'MAPK signaling pathway' (Fig. 9c). For the ME-medium purple-3 module, hub genes were predominantly enriched in 'methane metabolism', 'galactose metabolism', and 'valine, leucine, and isoleucine biosynthesis' (Fig. 9d).

To identify hub genes within each module, genes were ranked according to their module membership (kME values), and the top three genes with the highest connectivity were selected as hub genes for each module (Supplementary Table S2). In the ME-cyan module, the three identified hub genes were *Zs00007568*, *Zs00027633*, and *Zs00039195*. Notably, all three hub genes in this module belong to the heat shock protein/chaperone family. For the ME-yellow green module, the hub genes were *Zs00026862*, *Zs00007356*, and *Zs00027318*. These genes are predominantly involved in the biosynthesis and modification of cell wall components, including chitin-like polymers, glucomannan, and pectin. In the ME-dark turquoise module, the hub genes comprised *Zs00022285*, *Zs00031778*, and *Zs00032726*. The former two are key regulatory components of the jasmonic acid (JA) signaling pathway; the latter is a JA biosynthetic enzyme. The ME-medium purple-3 module contained *Zs00022799*, *Zs00026296*, and *Zs00037532* as its hub genes.

Discussion

Salt–alkali stress is one of the major global factors constraining crop growth and development[26]. Consequently, the mechanisms underlying plants' responses to such stress have remained a focal point of research[27]. Ginger, as an economically important crop, exhibits significant variation in salt–alkali tolerance, which directly influences its cultivation potential on saline–alkali soils. Under salt–alkali stress, plants typically mitigate damage by maintaining photosynthetic stability, enhancing osmotic adjustment, and bolstering antioxidant defenses[28].

In the present study, the decreases in chlorophyll *a*, chlorophyll *b*, and carotenoid contents were significantly greater in Ss (the sensitive cultivar under stress) compared with Ts (the tolerant cultivar under stress). Furthermore, the P_n, G_s, T_r, and WUE declined drastically in Ss, whereas C_i increased markedly. These results suggest that photosynthetic inhibition in Ss may have progressively shifted from being primarily stomatal in the early stages to predominantly nonstomatal. This finding aligns with results reported by Qiu et al. in soybean (*Glycine max*) under salt stress[29]. Salt–alkali stress induced increased amplitudes in the O–J and J–I phases of the OJIP curve in both cultivars, with the amplitudes being substantially higher in the sensitive cultivar (S) compared with the tolerant cultivar (T). This is likely attributable to the inhibition of electron transport in Photosystem II (PSII) and the consequent reduction in or even inactivation of reaction centers' activity[30]. Stress significantly elevated the V_k and V_j values in both cultivars, with the increases being more pronounced in the sensitive cultivar, S. This indicates severe inactivation of the oxygen-evolving complex (OEC) and a pronounced inhibition of electron donation on the donor side of in S under salt–alkali stress[31]. Although both cultivars exhibited significant declines in F_v/F_m and Y(II) under stress, the inhibition was more pronounced in the sensitive cultivar, which could be attributed to extensive degradation and denaturation of PSII reaction center proteins[32]. Compared with S, the tolerant cultivar, T, showed a significantly higher Y(NPQ) and markedly greater qP, suggesting that the salt–alkali-tolerant cultivar may cope with salt–alkali stress by initiating regulated energy dissipation and activating photoprotective mechanisms[33].

Osmotic adjustment is a central mechanism by which plants alleviate the water deficit induced by salt–alkali stress[15]. This study revealed significant differences in the accumulation patterns of osmolytes between the two cultivars. The salt–alkali-tolerant cultivar, T, rapidly and substantially accumulated proline, soluble sugars, and soluble proteins during the early stages of stress, maintaining these elevated levels throughout the stress period. Proline serves not only as a key compatible solute for maintaining cellular osmotic balance but also functions in stabilizing macromolecular structures and scavenging ROS[34]. Its sustained high accumulation is

https://doi.org/10.48130/vegres-0026-0030

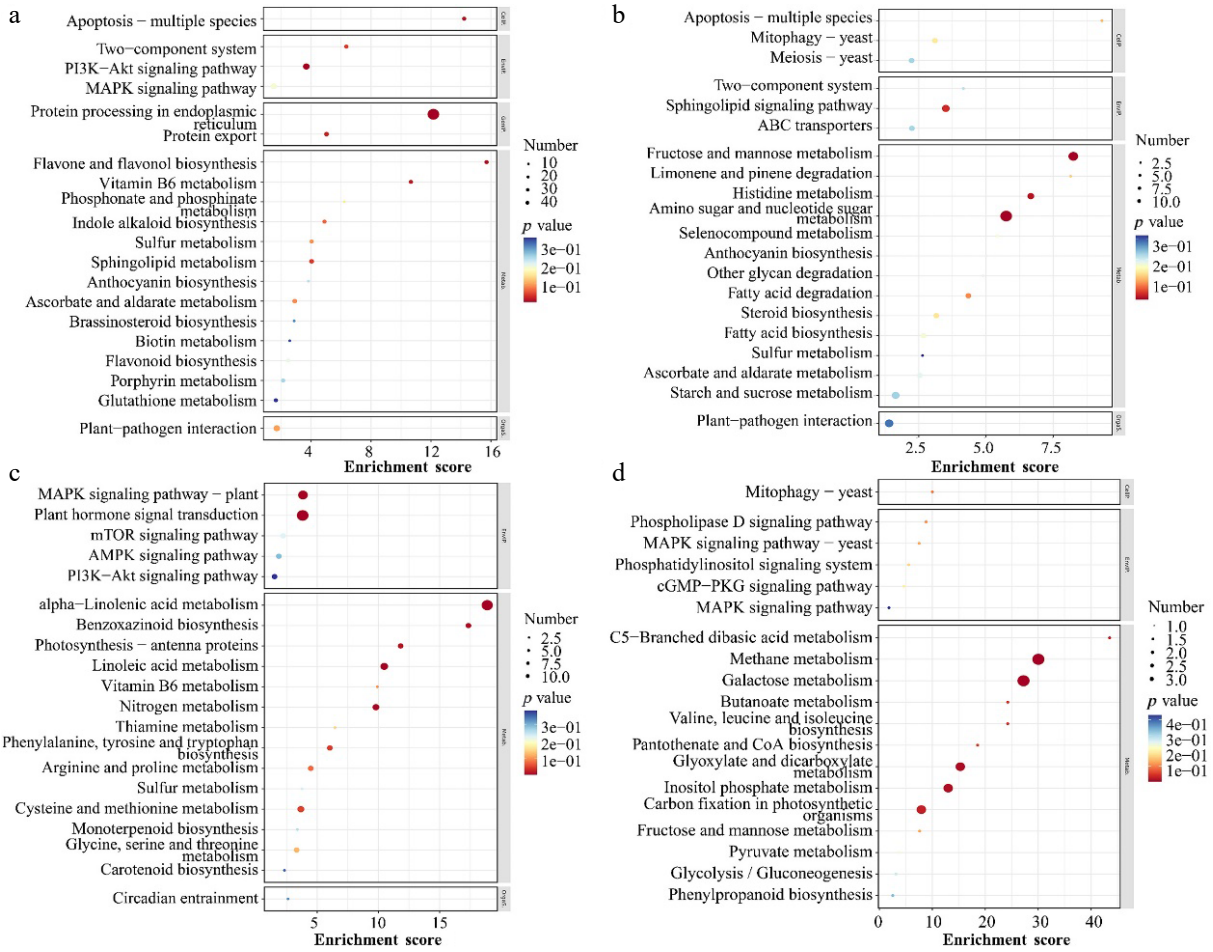


Fig. 9 KEGG enrichment analysis of key genes in four key modules. (a) ME-cyan module. (b) ME-yellow green module. (c) ME-dark turquoise module. (d) ME-medium purple-3 module.

indicative of T's proactive adaptation to the stressful environment. Similar studies have reported that salt–alkali-tolerant maize (*Zea mays*) lines accumulate far higher levels of proline, soluble sugars, and soluble proteins compared with sensitive lines under stress[35]. In contrast, the proline and soluble sugar contents in the sensitive cultivar showed only a transient increase during the initial stress phase before declining, and its soluble protein content decreased continuously. This disparity in accumulation patterns suggests that Cultivar S likely fails to sustain long-term, effective osmotic adjustment, leading to an earlier onset of cellular water imbalance and exacerbating physiological metabolic dysfunction[8]. Therefore, the efficient and sustained synthesis and accumulation of osmolytes represents a key physiological characteristic distinguishing salt–alkali-tolerant ginger cultivars from sensitive ones.

Osmotic stress and ion toxicity induced by salt–alkali conditions typically trigger secondary oxidative stress, leading to excessive accumulation of ROS[36]. This, in turn, causes membrane lipid peroxidation, protein denaturation, and damage to photosynthetic structures[37]. In this study, the contents of H_2O_2 and O_2^- increased over time in both cultivars under stress. However, the accumulation was significantly higher in the sensitive cultivar than in the tolerant cultivar, indicating that S suffered more severe oxidative damage. This is closely related to the impaired photosynthetic electron transport observed in S, as the decline in photosynthetic efficiency directly disrupts the balance between light energy capture and utilization. Excess excitation energy is then transferred to molecular oxygen, triggering a burst of ROS generation[38]. Consistent with this, Zhang et al. also reported that salt-tolerant cultivars exhibit lower ROS accumulation[14]. The MDA content increased in both cultivars following salt–alkali stress, aligning with the findings by Wang et al.[39]. In the tolerant cultivar, MDA levels increased gradually and then plateaued, whereas in the sensitive cultivar, MDA content continued to rise throughout the entire stress period. This may be attributed to the unmitigated oxidative damage to cell membranes in the sensitive cultivar, which ultimately resulted in irreversible membrane lipid peroxidation[40].

Faced with stress-induced ROS accumulation, plants rely on enzymatic and nonenzymatic antioxidant systems for scavenging[41]. In this study, the salt–alkali-tolerant cultivar established a more efficient and coordinated defense system. Regarding the enzymatic system, the activities of SOD, POD, CAT, and GR in T increased rapidly and remained elevated from the early stages of stress, forming a complete ROS-scavenging cascade. Similarly, Abdelrady et al.[42] observed that barley (*Hordeum vulgare*) enhances antioxidant enzyme activities to reduce ROS accumulation and adapt to stressful environments. In terms of the nonenzymatic system, Cultivar T maintained significantly higher levels of GSH and a higher GSH/GSSG ratio. GSH serves not only as a crucial antioxidant molecule but also as a substrate for GR and a key component of the ASA–GSH (Ascorbate-glutathione cycle) cycle. Its highly reduced

state is vital for maintaining cellular redox homeostasis[43]. Consequently, the synchronous enhancement of both enzymatic and non-enzymatic systems in T created a positive feedback loop, effectively controlling ROS levels and mitigating membrane lipid peroxidation. This, in turn, helped protect the structural integrity of organelles such as photosynthetic membranes, thereby contributing to the partial maintenance of photosynthetic function. In contrast, the antioxidant enzyme activities in the sensitive cultivar exhibited the pattern of an initial rise followed by a decline, indicating an insufficient response. Concurrently, its GSH pool was nearly depleted. This resulted in inadequate ROS-scavenging capacity, exacerbating oxidative damage and ultimately leading to severe leaf injury and even plant death.

To systematically dissect the coordinated involvement of enriched pathways in the saline–alkali tolerance of ginger, we combined correlation matrix analysis with PCA on physiological datasets. The photosynthetic module displayed tight internal correlations, whereas the oxidative damage module showed strong positive intercorrelations but negative associations with the photosynthetic parameters. Tolerant cultivars oriented toward the proline–antioxidant enzyme space, whereas sensitive cultivars shifted toward the oxidative damage space, revealing fundamental disparities in pathway orchestration underlying differential salt tolerance. Fan et al. similarly reported that photosynthetic decline was significantly negatively correlated with membrane oxidative damage (MDA), and that the basis of salt tolerance in poplar (*Populus* spp.) lies in the synergistic protective mechanism mediated by the coordinated action of antioxidant enzymes in ROS scavenging and the accumulation of osmotic regulators[44].

GO enrichment analysis revealed that the DEGs in both ginger cultivars under salt–alkali stress were significantly enriched in the 'response to abiotic stress' and 'photosynthetic membrane' terms. However, genes related to 'inorganic anion transmembrane transporter activity' and 'dicarboxylic acid transmembrane transporter activity' were more prominent in the tolerant cultivar. Under salt–alkali stress, plants primarily rely on the Salt Overly Sensitive pathway and the NHX family to extrude or compartmentalize excess Na^+, while also maintaining Cl^- and anion balance[45]. In this study, the enrichment of these transporter-related GO terms in the tolerant cultivar may reflect more efficient ion compartmentalization. Importantly, the significant enrichment of 'dicarboxylic acid transmembrane transporter activity' terms in the tolerant genotype was closely linked to malate translocation[46]. Cytosolic malate is oxidatively decarboxylated by malic enzyme (ME) to produce nicotinamide adenine dinucleotide phosphate (NADPH), which serves as the essential electron donor for GR-mediated regeneration of GSH from GSSG, ensuring the robust functioning of antioxidant enzymes including GR and DHAR under saline stress[47]. This provides a direct molecular explanation for the elevated GSH/GSSG ratio and diminished ROS levels observed in T.

KEGG enrichment analysis identified three pathways significantly enriched in both cultivars: 'Metabolism of xenobiotics by cytochrome P450', 'alpha-linolenic acid metabolism', and 'ferroptosis'. Ferroptosis buildup was closely linked to the continuous rise of MDA and H_2O_2, pointing to irreversible oxidative cell death. On the other hand, in Cultivar T, this pathway was only triggered temporarily, and MDA levels stabilized after Day 5, suggesting it acts more like a stress alert signal that is later controlled by a strong GSH-based antioxidant system. Li and colleagues saw similar results in salt-stressed *A. thaliana* roots[48]. Previous studies have linked 'alpha-linolenic acid metabolism' to various abiotic stresses[49]. In this study, the co-enrichment of the two varieties may be associated with the opposing expression profiles of the relevant genes. Regarding cultivar-specific enrichment, Cultivar T showed enrichment in pathways such as 'thiamine metabolism' and 'methane metabolism'. The product of the 'thiamine metabolism' pathway, thiamine, serves as a cofactor for key enzymes in both carbohydrate metabolism and the pentose phosphate pathway[50], and its upregulation may thus support the sustained sugar accumulation observed in T. However, the biological significance of 'methane metabolism' in the leaf response of ginger to salt–alkali stress currently lacks support in the literature and may reflect broad metabolic disturbances, warranting further investigation. Cultivar S was enriched in pathways including 'glycerolipid metabolism', 'galactose metabolism', and 'photosynthesis – antenna proteins'. The co-enrichment of these pathways, coupled with the decrease in Y(II) and chlorophyll content, strongly suggests a transcriptional signature indicative of thylakoid membrane disassembly and photosynthetic complex degradation. Specifically, the enrichment of the 'galactose metabolism' pathway likely reflects an active breakdown of galactolipids, the predominant lipid class in thylakoid membranes[51], thereby providing a molecular explanation for the severe chloroplast structural damage inferred from chlorophyll fluorescence imaging.

Through WGCNA analysis, we identified three positively associated with Cultivar T: ME-cyan, ME-yellow green, and ME-dark turquoise. ME-cyan module (Day 1) was enriched in 'protein processing in endoplasmic reticulum', with *HSP70* (*Heat shock 70-kDa protein 15*) serving as the hub gene. Under salt-induced endoplasmic reticulum (ER) stress, *HSP70* functions as a key player in the unfolded protein response (UPR) by facilitating correct protein folding and thereby suppressing the accumulation of misfolded protein aggregates[52]. This early chaperone-mediated protective response precedes the accumulation of osmoprotective solutes, suggesting that the defense strategy of the tolerant genotype is temporally layered. The ME-yellow green module (Day 5) was enriched in 'amino sugar and nucleotide sugar metabolism' as well as 'fructose and mannose metabolism'. The hub DEGs included *CSLA9* (*glucomannan 4-beta-mannosyltransferase*) and *GAUT8* (*Galacturonosyltransferase 8*). Previous studies have shown that members of the glycosyltransferase family to which *CSLA9* belongs can be induced to upregulate under salt stress, and it is speculated that they may enhance the mechanical properties of the cell wall by promoting the synthesis and remodeling of cell wall polysaccharides, thereby alleviating damage caused by osmotic stress[53]. Given its role in pectin biosynthesis, *GAUT8* is postulated to reinforce cell walls' mechanical integrity and maintain cell-to-cell adhesion through the synthesis and remodeling of pectin, thus mitigating osmotic stress-induced injury under saline–alkali conditions[54]. The concomitant upregulation of *CSLA9* and *GAUT8* in the tolerant cultivar is indicative of a mechanism that strengthens the cell wall architecture and preserves intercellular adhesion, thus preventing the collapse of mesophyll tissue under saline–alkali stress. Such structural fortification is expected to indirectly facilitate stomatal movement and CO_2 conductance, given that guard cells' biomechanics are critically influenced by the cell walls' mechanical properties[55]. The physiological basis of this interpretation is further substantiated by the higher G_s and P_n values in Cultivar T. In addition, the temporal coincidence of *CSLA9*/*GAUT8* upregulation with the maximal soluble sugar content in T implies that surplus photosynthates are redirected to strengthen the cell wall, which may function as a physical barrier restricting ionic intrusion. In our study, the ME-dark turquoise

module (Day 7) was enriched in 'plant hormone signal transduction' and 'MAPK signaling pathway'. The hub DEGs included *bHLH148* (*transcription factor BHLH148*), *TIFY* (*transcription factor TIFY*), and *AOC* (*allene oxide cyclase*), indicating that the JA signaling module plays an important role in saline–alkali tolerance in ginger[56]. The concomitant upregulation of *TIFY* and *AOC* in the tolerant cultivar is indicative of a negative feedback mechanism, wherein JA synthesis initiates a self-amplifying signaling cascade while simultaneously inducing *TIFY* to constrain excessive activation. Such a regulatory architecture likely ensures a temporally restricted and precisely calibrated defense output, as opposed to a prolonged and metabolically expensive stress response[57,58]. The module eigengenes of the ME-dark turquoise module were closely correlated with CAT and GR activities, supporting a mechanism by which JA signaling orchestrates a phosphorylation-dependent transcriptional cascade. This mechanism establishes a negative feedback loop to attenuate the oxidative burst, thereby safeguarding the photosynthetic electron transport chain. Notably, in the sensitive cultivar, the JA module failed to be activated, resulting in uncontrolled ROS accumulation and a 40.13% increase in MDA content by Day 10 (Fig. 4a).

On the basis of the abovementioned analyses, nine hub genes were prioritized as the most promising candidate targets for future functional characterization in ginger. The temporal expression patterns of these genes collectively delineate a hierarchical regulatory framework for saline–alkali tolerance, encompassing ER chaperone-mediated protein quality control in the early stress phase, cell wall carbohydrate biosynthesis in the intermediate phase, and JA-mediated ROS homeostasis in the late phase. In contrast, the sensitive cultivar fails through temporal decoupling of these phases, ultimately succumbing to ferroptotic cell death. This model provides a systems-level roadmap for understanding salt–alkali tolerance in ginger, emphasizing that breeding efforts should prioritize the coordinated rewiring of these time-dependent regulatory modules rather than focusing on single 'super genes'.

Conclusions

This study demonstrates that the salt–alkali-tolerant ginger cultivar, T, copes with stress through a series of physiological and molecular strategies, including maintaining the relative stability of photosynthetic structure and function, efficiently accumulating osmolytes to alleviate osmotic stress, scavenging ROS via both enzymatic and nonenzymatic pathways to mitigate membrane lipid peroxidation, and initiating transcriptional reprogramming involving pathways related to ion transport, osmotic adjustment, antioxidation, hormone signaling, and MAPK cascades. In contrast, the sensitive cultivar, S, exhibits varying degrees of deficiency or dysregulation in its responses at the abovementioned levels. This study mainly analyzed the physiological differences and candidate coexpression modules between the two cultivars under salt–alkali stress. Nine hub genes were screened, providing potential genetic resources for future stress-resistant genetic improvement and the creation of superior germplasm resources in ginger.

Author contributions

The authors confirm their contributions to this study as follows: writing – original draft, methodology, investigation, visualization: Liu H; data curation, formal analysis: Gao S, Chen Z; resources, validation: Wang D, Liu M; software, investigation: Kong Y, Li X, Ai J; writing – review and editing, funding acquisition: Lv Y; supervision, project administration, funding acquisition: Xu K. All authors reviewed the results and approved the final version of the manuscript.

Data availability

Sequence data have been deposited in the NCBI Sequence Read Archive (SRA) database (PRJNA1459671).

Acknowledgments

We thank Ke Liu (USA) for English language editing of this manuscript. This study was supported by the Agricultural Fine Variety Project in Shandong Province of China (Grant No. 2023LZGCQY003), the National Key Research and Development Program of China (Grant No. 2023YFD1600202), China Agriculture Research System (Grant No. CARS-24-A-09), the National Natural Science Foundation of China (Grant No. 32302530), and the Young Talent of Lifting Engineering for Science and Technology in Shandong, China (SDAST2024QTA016).

Conflict of interest

The authors declare that they have no conflict of interest.

Supplementary information accompanies this paper online at https://doi.org/10.48130/vegres-0026-0030.

Dates

Received 12 March 2026; Revised 13 July 2026; Accepted 12 August 2026; Published online 30 October 2026

References

[1] Guo S, Chen Y, Ju Y, Pan C, Shan J, et al. 2025. Fine-tuning gibberellin improves rice alkali–thermal tolerance and yield. *Nature* 639:162–171

[2] Xiang G, Fan Z, Lan S, Wei D, Gao Y, et al. 2025. Ethylene increases the $NaHCO_3$ stress tolerance of grapevines partially via the VvERF1B-$VvMYC_2$-VvPMA10 pathway. *Plant Biotechnology Journal* 23:1076–1090

[3] Liu H, Liu Q, Hepworth SR, Li P, Huang J, et al. 2025. ZxNHX1 from a xerophyte outperforms AtNHX1 in sequestering Na+ into vacuoles to enhance plant stress resistance and yield. *Plant Biotechnology Journal* 23:3497–3509

[4] Yin F, Lv Y, Cao B, Zhang S, Xu K. 2024. Physiological and transcriptomic investigation of low pH-mediated salt stress alleviation in ginger (*Zingiber officinale* Rosc.). *Scientia Horticulturae* 331:113101

[5] Ren H, Zhang B, Zhang F, Liu X, Wang X, et al. 2024. Integration of physiological and transcriptomic approaches in investigating salt–alkali stress resilience in soybean. *Plant Stress* 11:100375

[6] Wang H, An T, Huang D, Liu R, Xu B, et al. 2021. Arbuscular mycorrhizal symbioses alleviating salt stress in maize is associated with a decline in root-to-leaf gradient of Na^+/K^+ ratio. *BMC Plant Biology* 21:457

[7] Yan N, Wang W, Mi T, Zhang X, Li X, et al. 2024. Enhancing tomato growth and soil fertility under salinity stress using halotolerant plant growth-promoting rhizobacteria. *Plant Stress* 14:100638

[8] Liu M, Gao J, Wang N, Yan Y, Zhang G, et al. 2024. Effects of exogenous GABA on physiological characteristics of licorice seedlings under saline–alkali stress. *Plant Stress* 11:100364

[9] Jia X, Wang H, Svetla S, Zhu Y, Hu Y, et al. 2019. Comparative physiological responses and adaptive strategies of apple Malus halliana to salt, alkali and saline–alkali stress. *Scientia Horticulturae* 245:154–162

[10] Agha MS, Haroun SA, Abbas MA, Sofy MR, Mowafy AM. 2023. Growth and metabolic response of *Glycine max* to the plant growth-promoting *Enterobacter* Delta PSK and *Bradyrhizobium japonicum* under salinity stress. *Journal of Plant Growth Regulation* 42:5816−5830

[11] Hua Y, Pei M, Song H, Liu Y, Zhou T, et al. 2024. Boron confers salt tolerance through facilitating BnaA2. HKT1-mediated root xylem Na^+ unloading in rapeseed (*Brassica napus* L.). *The Plant Journal: for cell and molecular biology* 120:1326−1342

[12] Han G, Yuan F, Guo J, Zhang Y, Sui N, et al. 2019. AtSIZ1 improves salt tolerance by maintaining ionic homeostasis and osmotic balance in Arabidopsis. *Plant Science* 285:55−67

[13] Liu X, Shang C, Duan P, Yang J, Wang J, et al. 2025. The SlWRKY42-$SlMYC_2$ module synergistically enhances tomato saline-alkali tolerance by activating the jasmonic acid signaling and spermidine biosynthesis pathway. *Journal of Integrative Plant Biology* 67:1254−1273

[14] Zhang C, Jiang K, Liu Q, Xu H, Ning K, et al. 2025. Screening of salt-tolerant soybean germplasm and study of salt-tolerance mechanism. *Plant Cell Reports* 44:187

[15] Chen S, Zhou Q, Feng Y, Dong Y, Zhang Z, et al. 2024. Responsive mechanism of Hemerocallis citrina Baroni to complex saline-alkali stress revealed by photosynthetic characteristics and antioxidant regulation. *Plant Cell Reports* 43:176

[16] Xu Z, Liu Y, Zhao Y, Song X, Zhu Y, et al. 2024. R2R3-MYB transcription factor $GmMYB_6$8 is involved in the accumulation of soybean isoflavones. *Plant Physiology and Biochemistry* 216:109187

[17] Chen Z, Zhang L, Lv Y, Qu S, Liu W, et al. 2024. A genome assembly of ginger (*Zingiber officinale* Roscoe) provides insights into genome evolution and 6-gingerol biosynthesis. *The Plant Journal* 118:682−695

[18] Gao D, Ran C, Zhang Y, Wang X, Lu S, et al. 2022. Effect of different concentrations of foliar iron fertilizer on chlorophyll fluorescence characteristics of iron-deficient rice seedlings under saline sodic conditions. *Plant Physiology and Biochemistry* 185:112−122

[19] Wang D, Wang J, Wang K, Lv Y, Xu K. 2024. Mechanisms of UHP alleviates waterlogging-induced damage in ginger (*Zingiber officinale*). *Scientia Horticulturae* 332:113190

[20] Liu S, Sun B, Cao B, Lv Y, Chen Z, et al. 2023. Effects of soil waterlogging and high-temperature stress on photosynthesis and photosystem II of ginger (*Zingiber officinale*). *Protoplasma* 260:405−418

[21] Shi L, Dong X, Fu H, Chai X, Bao S, et al. 2023. Differences in physiological characteristics of green prickly ash germplasm resources in response to low-temperature stress. *Horticulturae* 9:1242

[22] Li X, Li R, Wang K, Kong Y, Lv Y, et al. 2025. Physiological mechanism of Welsh onion (*Allium fistulosum* L.) in response to high temperature and waterlogging stress. *Agronomy* 15:482

[23] Zafari S, Sharifi M, Ahmadian Chashmi N, Mur LAJ. 2016. Modulation of Pb-induced stress in Prosopis shoots through an interconnected network of signaling molecules, phenolic compounds and amino acids. *Plant Physiology and Biochemistry* 99:11−20

[24] Guo W, Chen R, Gong Z, Yin Y, Ahmed SS, et al. 2012. Exogenous abscisic acid increases antioxidant enzymes and related gene expression in pepper (*Capsicum annuum*) leaves subjected to chilling stress. *Genetics and Molecular Research* 11:4063−4080

[25] Lv Y, Li Y, Liu X, Xu K. 2020. Identification of ginger (*Zingiber officinale* Roscoe) reference genes for gene expression analysis. *Frontiers in Genetics* 11:586098

[26] Kazamel AM, Haroun SA, Noureldin AA, El-Sherbiny GA, El-Shahaby OA, et al. 2023. Ultrastructural, secondary metabolite, and antioxidant modulation in response to salt-affected habitats induced oxidative stress and their accumulation in *Malva parviflora* L. and *Rumex dentatus* L. *Journal of Soil Science and Plant Nutrition* 24:389−407

[27] Li J, Xu C, Tian Y, Chen G, Chi W, et al. 2025. Genome-wide association and selection studies reveal genomic insight into saline-alkali tolerance in rice. *The Plant Journal* 121:e70056

[28] Li N, Zhang Z, Gao S, Lv Y, Chen Z, et al. 2021. Different responses of two Chinese cabbage (*Brassica rapa* L. ssp. pekinensis) cultivars in photosynthetic characteristics and chloroplast ultrastructure to salt and alkali stress. *Planta* 254:102

[29] Qiu S, Zhang Y, Sun H, Liu L, Li C, et al. 2025. Integrated transcriptomics and metabolomics elucidate additive inhibitory effects of combined salinity-waterlogging stress on soybean growth and metabolic adaptations. *Plant Physiology and Biochemistry* 223:109847

[30] Wang X, Wang J, Yin J, Li J. 2022. Comparison of the physiological factors in ion accumulation and photosynthetic electron transport between legumes *Medicago truncatula* and *Medicago sativa* under salt stress. *Plant and Soil* 484:473−486

[31] Gao S, Kong Y, Lv Y, Cao B, Chen Z, et al. 2022. Effect of different LED light quality combination on the content of vitamin C, soluble sugar, organic acids, amino acids, antioxidant capacity and mineral elements in green onion (*Allium fistulosum* L.). *Food Research International* 156:111329

[32] Gao Y, Liu W, Wang X, Yang L, Han S, et al. 2018. Comparative phytotoxicity of usnic acid, salicylic acid, cinnamic acid and benzoic acid on photosynthetic apparatus of Chlamydomonas reinhardtii. *Plant Physiology and Biochemistry* 128:1−12

[33] Chen J, Tang L, Guo W, Wang D, Sun Y, et al. 2024. Oxalic acid secretion alleviates saline-alkali stress in alfalfa by improving photosynthetic characteristics and antioxidant activity. *Plant Physiology and Bochemistry* 208:108475

[34] Min Y, Yu D, Yang J, Zhao W, Zhang L, et al. 2023. Bioinformatics and expression analysis of proline metabolism-related gene families in alfalfa under saline-alkali stress. *Plant Physiology and Biochemistry* 205:108182

[35] Wang C, Wang Y, Cao X, Wu C, Wei X, et al. 2025. Unraveling saline-alkali stress tolerance: contrasting morpho-physiological, biochemical, and ionic responses in maize (*Zea mays* L.) genotypes. *Plant Physiology and Biochemistry* 229:110349

[36] Sakit ALHaithloul HA, Khan MI, Musa A, Ghoneim MM, Aysh ALrashidi A, et al. 2022. Phytotoxic effects of Acacia saligna dry leachates on germination, seedling growth, photosynthetic performance, and gene expression of economically important crops. *PeerJ* 10:e13623−e

[37] Lu X, Ma L, Zhang C, Yan H, Bao J, et al. 2022. Grapevine (*Vitis vinifera*) responses to salt stress and alkali stress: transcriptional and metabolic profiling. *BMC Plant Biology* 22:528

[38] Wan S, Zhang Y, Liu L, Xiao Y, He J, et al. 2024. Comparative effects of salt and alkali stress on photosynthesis and antioxidant system in tea plant (*Camellia sinensis*). *Plant Growth Regulation* 103:565−579

[39] Wang Y, Stevanato P, Yu L, Zhao H, Sun X, et al. 2017. The physiological and metabolic changes in sugar beet seedlings under different levels of salt stress. *Journal of Plant Research* 130:1079−1093

[40] Zhang X, Li S, Tang T, Liu Y, Mobeen Tahir M, et al. 2022. Comparison of morphological, physiological, and related-gene expression responses to saline-alkali stress in eight apple rootstock genotypes. *Scientia Horticulturae* 306

[41] Yi E, Zhang J, Jiang Y, Yang L, Sun M, et al. 2025. *Bacillus amyloliquefaciens* YB1701 enhances rice tolerance to saline-alkali stress *via* ROS scavenging and ion homeostasis. *Current Microbiology* 82:590

[42] Abdelrady WA, Ma Z, Elshawy EE, Wang L, Askri SMH, et al. 2024. Physiological and biochemical mechanisms of salt tolerance in barley under salinity stress. *Plant Stress* 11:100403

[43] Liu Y, Zheng J, Ge L, Tang H, Hu J, et al. 2024. Integrated metabolomic and transcriptomic analyses reveal the roles of alanine, aspartate and glutamate metabolism and glutathione metabolism in response to salt stress in tomato. *Scientia Horticulturae* 328:112911

[44] Fan L, Zhou Q, Yang H, Ling X, Fan W, et al. 2025. Effects of salt stress on the physiology and biochemistry of six poplar germplasms and evaluation of their salt tolerance. *Forests* 16:1733

[45] Guo H, Huang Z, Li M, Hou Z. 2020. Growth, ionic homeostasis, and physiological responses of cotton under different salt and alkali stresses. *Scientific Reports* 10:21844

[46] Wei X, Xu L, Dong S, He N, Xi Q, et al. 2024. SaTDT enhanced plant tolerance to NaCl stress by modulating the levels of malic acid and citric acid in cells. *Plant Molecular Biology* 115:4
[47] Chen Q, Wang B, Ding H, Zhang J, Li S. 2019. Review: the role of NADP-malic enzyme in plants under stress. *Plant Science* 281:206−212
[48] Li Z, Yan X, Dong J, Zhang H, Yang X, et al. 2026. Abolishment of N-glycan trimming in the early Golgi triggers ferroptosis under salt stress in *Arabidopsis* root tips. *New phytologist* 249:342−358
[49] Zaman S, Hu S, Alam MA, Du H, Che S. 2019. The accumulation of fatty acids in different organs of purslane under salt stress. *Scientia Horticulturae* 250:236−242
[50] Rapala-Kozik M, Wolak N, Kujda M, Banas AK. 2012. The upregulation of thiamine (vitamin B_1) biosynthesis in *Arabidopsis thaliana* seedlings under salt and osmotic stress conditions is mediated by abscisic acid at the early stages of this stress response. *BMC Plant Biology* 12:2
[51] Bai G, Zhang H, Li Y, Yang D, Fei M, et al. 2025. Integration of metabolic and transcriptomic analyses for revealing the galactose metabolism of tobacco (*Nicotiana tabacum*) under salt stress. *Frontiers in Plant Science* 16:1614515
[52] Fu Q, Pu Y, Liu J, Wang X, Li D, et al. 2025. Genome-wide analysis of the *DnaJ* gene family and their expression profiles under salt stress in potato. *BMC Genomics* 26:758
[53] Mota-Ituarte M, Quezada-Rivera J, Pedroza-Sandoval A, Saenz-Mata J, Minjares-Fuentes R. 2025. Key genes involved in the saline-water stress tolerance of aloe vera. *Current Issues in Molecular Biology* 47:1000
[54] Caffall KH, Pattathil S, Phillips SE, Hahn MG, Mohnen D. 2009. *Arabidopsis thaliana* T-DNA mutants implicate GAUT genes in the biosynthesis of pectin and xylan in cell walls and seed testa. *Molecular Plant* 2:1000−1014
[55] Yang Q, Yan X, Wang N, Zenda T, Dong A, et al. 2025. ZmWAK3-mediated cell wall remodeling and stomatal dynamics modulate drought tolerance in maize seedlings. *Theoretical and Applied Genetics* 138:249
[56] Seo JS, Joo J, Kim MJ, Kim YK, Nahm BH, et al. 2011. OsbHLH148, a basic helix-loop-helix protein, interacts with OsJAZ proteins in a jasmonate signaling pathway leading to drought tolerance in rice. *The Plant Journal* 65:907−921
[57] Zhu D, Bai X, Luo X, Chen Q, Cai H, et al. 2013. Identification of wild soybean (*Glycine soja*) TIFY family genes and their expression profiling analysis under bicarbonate stress. *Plant Cell Reports* 32:263−272
[58] Hofmann E, Pollmann S. 2008. Molecular mechanism of enzymatic allene oxide cyclization in plants. *Plant Physiology and Biochemistry* 46:302−308

Copyright: © 2026 by the author(s). Published by Maximum Academic Press, Fayetteville, GA. This article is an open access article distributed under Creative Commons Attribution License (CC BY 4.0), visit https://creativecommons.org/licenses/by/4.0/.